COOLING FLOW MODELS OF THE X–RAY EMISSION AND TEMPERATURE PROFILES FOR A SAMPLE OF ELLIPTICAL GALAXIES

G. Bertin and T. Toniazzo

Scuola Normale Superiore, Piazza dei Cavalieri 7, I 56126, Pisa, Italy

ABSTRACT

A simple spherically-symmetric, steady-state, cooling-flow description with gas loss (following Sarazin & Ashe 1989), within galaxy models constrained by radially extended stellar dynamical data, is shown to provide generally reasonable fits to the existing data on X-ray emission profiles and temperatures for a set of bright elliptical galaxies in Virgo and Fornax. Three free parameters are needed to specify the model: the external mass flux, the external pressure, and a dimensionless factor, which regulates the mass deposition rate along the flow. Three different assumptions on the supernova rate have been considered. A moderate value for the supernova rate in elliptical galaxies is found to be preferred. Confining pressures of $p_{ext} \sim 4 \div 15 \times 10^3$ ^{0}K cm^{-3} and significant accretion rates of external material, up to $4 M_\odot$/yr, are suggested by our models. A possible correlation between L_X/L_B and the iron abundance in the gas inside ellipticals is pointed out.

Subject headings:

Galaxies: Cooling Flows – Galaxies: Elliptical and Lenticular, cD – Galaxies: Intergalactic Medium – Galaxies: ISM – Galaxies: Structure – X-Rays: Galaxies

1. INTRODUCTION

In their simplest form, cooling flow models for the description of the X–ray emission from individual galaxies (see Sarazin and White 1987, Vedder, Trester, and Canizares 1988) have a history of mixed success (see Sarazin 1990 and references therein).

On the one hand, a steady state description of the dynamics of the hot interstellar medium may be too naive, in view of the expected time dependence of the basic energy balance during galaxy evolution (see Loewenstein and Mathews 1987, David, Forman, and Jones 1990, Ciotti et al. 1991, Binney and Tabor 1995). In this respect, as with several examples in other physical contexts, one argues that the time scale of the overall evolution of the system that is considered is sufficiently long that a simple steady state analysis can correctly capture the properties of at least some of the stages of the time evolving hot gas, and, in particular, that the steady state cooling "inflow" description gives a reasonable representation of the current state of the brightest X-ray ellipticals. Attempts have been made to check in detail what are the conditions for the applicability of the steady state description through examination of the results of hydrodynamical codes (Murray and Balbus 1992).

On the other hand, it was immediately realized that the simplest cooling flow models all suffered from a basic inconsistency with the observations in that, given the piling up of hot gas, the theoretically predicted emission profiles are too bright close to the galaxy center (see Sarazin and White 1988). Various ways have been proposed to correct the cooling flow model in order to resolve the problem of the excessive steepness of the surface brightness profile, by recognizing that part of the hot gas is bound to decouple away from the cooling flow (Thomas 1986, Thomas et al. 1986, Sarazin and Ashe 1989). To some extent, the filamentary structure of the gas noted earlier especially around cD's (e.g., see Lynds 1970) and dramatically demonstrated on the cluster scale by recent *Rosat* observations (Sarazin, O'Connell, and McNamara 1992a,b) adds further encouragement in this direction. One might even conclude that some of these observations undermine the very foundation of the simple spherical, steady state, one–phase cooling flow as a model for the hot gas.

The impact of the constraints posed by stellar dynamical data on the modeling of the X–ray emitting gas in elliptical galaxies was examined in a previous paper (Bertin, Pignatelli, and Saglia 1993; hereafter BPS). This paper focused on the problem of dark matter and on the galaxy NGC 4472, for which radially extended optical spectroscopic profiles are available (Saglia et al. 1993). Such a study gave one surprising result and confirmed one well known fact. The surprise was to find that the predicted temperature and surface brightness profiles for the hot gas for models with or without significant amounts of dark matter, if constrained by the same set of stellar dynamical data out to $\approx R_e$ (the *effective* optical radius), are very similar to each other even out to $\approx 7R_e$; in particular, the temperature profiles are found to be much more sensitive to the assumed value of the intracluster pressure p_{ext} than to the amount of dark matter that may be argued to be present. This surprising result urges caution in the use of X–ray data as diagnostics for the presence of dark halos (see Loewenstein 1992 and Serlemitsos et al. 1993). The well known fact confirmed by the analysis of BPS is the central overbrightness problem for the simplest form of cooling flow models of the hot gas: the case of NGC 4472 shows that the use of accurate models for the distribution of the stellar component can only lead to a slight improvement of the predicted X–ray emission profile, which remains too steep and definitely fails at $R \leq 0.2R_e$.

In this paper we continue the study started by BPS, by focusing on the modeling of the X–ray emitting gas for galaxies for which accurate stellar dynamical models are available. In doing so, we may have confidence in the adopted profiles for the functions $\rho_\star(r)$ and $\sigma_\star(r)$, that characterize the stellar density and velocity dispersion profiles, and for the gravitational potential $\Phi(r)$. In view of the study of BPS, here we omit further discussions on the role of dark matter and simply refer to the available best fit stellar dynamical models (which include, in general, a dark halo). The main goal of this paper is then to test the adequacy of simple steady state, spherical

cooling flow models for the hot gas by studying in detail the role of the decoupling of cold gas from the flow, following the prescription of Sarazin and Ashe (1989), and the role of the intracluster medium. The analysis thus basically relies on the variation of three parameters (q, p_{ext}, and $\dot{m}_{ext}$; see §3 below). Qualitatively, the effects of these variations are well known (see papers cited above). Here we would like to make a full detailed quantitative test in order to ascertain whether a simple uniform choice for q and physically plausible properties of the intracluster medium can lead to good fits to the X–ray emission profiles and to the temperature profiles (if available) for several objects.

As noted earlier (e.g., see discussion in §2 of BPS), the presence of a finite pressure at the outer boundary is associated with the existence of an inflow of gas from the cluster. Furthermore, for some objects (like NGC1399 and NGC4636 in our sample, see §4), a significant rate of accretion from the cluster, exceeding the value of $1M_{\odot}$/yr, is found to be required in the present frame of steady–state cooling flows. Therefore, in this paper, as will be described in the following §3, we solve the relevant equations treating the outer boundary differently from Vedder et al. (1988) and BPS, in that we consider the possibility of an inflow of extragalactic matter as a separate parameter ($\dot{m}_{ext}$), in addition to the pressure at the external boundary p_{ext}, to be adjusted in the fit process. For galaxies with a low value of L_X/L_B for which no significant accretion is required, in order to avoid the formal singular behavior of the solution which would be associated with the so–called stagnation radius (introduced as the radius where the radial velocity of the flow vanishes), we set $\dot{m}_{ext} = 0.1M_{\odot}$/yr. When the accretion rate is so low, the resulting profiles are hardly affected by the precise value of $\dot{m}_{ext}$.

The physics of the hot gas is intrinsically complex. In this paper we focus on three factors of the problem, on the basis of their physical interest. The first factor is the decoupling of cold gas from the hot inflow. The mass decoupling term introduced by Sarazin and Ashe (1989) provides a phenomenological description (with one free parameter, called q) of the consequences of small-scale fluid instabilities which are expected to take place in the cooling gas (although different views can be taken on the issue; see Fabian and Nulsen 1977, Mathews and Bregman 1978, Balbus 1988, Loewenstein 1989, 1990). Therefore, it would be desirable that the fitting value of q be of order unity, with small variations from one galaxy to another, and that the model profiles turn out to be not too sensitive to q in the vicinity of the best fit value. The second factor is the role of the external pressure, which can be constrained, to some extent, by direct observations of the intracluster plasma. By considering galaxies in the same cluster, i.e. embedded in the same intracluster medium, one can better appreciate whether the adopted values of p_{ext} and $\dot{m}_{ext}$ are physically plausible. Ideally, besides studying the case of different clusters (as is done below), it would be very interesting to model truly isolated X–ray bright ellipticals; unfortunately, such a case is not easy to find. The third physical factor of the problem addressed in the present analysis is related to the determination of the supernova Ia rate in ellipticals. The cooling flow models found in this paper appear to give better fits to the data if a value is used consistent with the recent estimates of Cappellaro et al. (1993).

Even if the set of objects modeled in this paper is very small, the results of the fits performed here (§4) are of considerable interest. It is found that reasonable fits are obtained with a reasonable choice of the parameters involved, *even if the models used are highly idealized*. Furthermore, if we consider that the data on X–ray temperature "profiles" used here are very crude (with the exception of the *Rosat* data for NGC 4636, taken from Trinchieri et al. 1994), and that the reduction of X-ray spectroscopic data and their interpretation usually leave several options open (that is, the choice of the parameters to be used in the fit such as chemical composition, HI absorption, and number of emitting components involved; see Trinchieri et al. 1994 and Pellegrini & Fabbiano 1994), we may take the theoretical models produced in this paper as "predictions" against the better temperature profiles that are currently being gathered with the help of new telescopes and instruments.

2. THE SAMPLE.

The galaxies that define our sample have been selected on the basis of the following criteria: (i) High X-ray luminosity, (ii) Availability of good quality X-ray data, (iii) Availability of good quality stellar dynamical data and of detailed global stellar dynamical models. Criterion (i) is related to our plan to model the X-ray emission and temperature profiles in terms of cooling flows; this is justified only for objects with high L_X/L_B (see, e.g., Ciotti et al. 1991). In relation to point (ii), we have referred to the X-ray contour maps and circularized surface brightness profiles given in the *Einstein* X-ray catalogue of Fabbiano, Kim & Trinchieri (1992), in order to pick out galaxies with high signal, extended X-ray halos. Requirement (iii) allows us to perform a study of the coronal gas within an accurately determined potential well and a detailed quantitative framework for the properties of the stellar component. For this latter purpose we have made use of the results of the survey of Saglia, Bertin, and Stiavelli (1992; hereafter SBS).

The sample of selected objects thus contains 5 galaxies: NGC 1399, NGC 1404, NGC 4374, NGC 4472, and NGC 4636. Their optical and X-ray properties are listed in Table 1. All the galaxies selected are fairly round in their optical appearance (this was indeed one of the main criteria for the selection of the sample of SBS), which makes the use of spherical models at least a reasonable starting point. The last four columns of Table 1 describe some X-ray properties of the galaxies, taken from the literature. The radius R_X denotes the radius of the X-ray emitting region considered by each source, and L_X is the total X-ray flux from within R_X. The seventh column is the best-fit temperature of a single-component Raymond thermal spectrum fitted to the region considered, and can thus be taken as an estimate of an average temperature of the gas within R_X. Finally, it should be noted that the reported total X-ray fluxes in the specified bands are highly dependent on the assumed hydrogen column density along the line-of-sight. Fabbiano et al. (1992) estimate the count/energy conversion factor by assuming a gas temperature of 1 keV and galactic absorption.

The available X-ray emission profiles of NGC 1399, NGC 4472, and NGC 4636 considered in this paper are quite accurate. We refer to IPC data for NGC 1399, combined IPC/HRI data for NGC 4472 and *Rosat* PSPC data for NGC 4636. Temperature determinations are taken from Serlemitsos et al. (1993; *BBXRT* data for NGC 1399 and NGC 4472), Forman, Jones, and Tucker (1985; *Einstein* IPC data for NGC 4472) and Trinchieri et al. (1994; *Rosat* PSPC data for NGC 4636).

NGC 1404 is embedded in the very extended bright halo of NGC 1399. Thus the X-ray total luminosity and the emission profile for NGC 1404 may suffer from subtraction problems; furthermore, the temperature determination is rather uncertain, given the low energy resolution of the IPC instrument (see Kim, Fabbiano & Trinchieri 1992). Similar problems might affect the X-ray properties reported for NGC4374 (which is near NGC 4406), although HRI data are also available for this object. Some of these uncertainties might be resolved with the help of *Rosat* data, when analyses of these data have been published.

NGC 1399 and NGC 1404 are at the center of the Fornax cluster, while the remaining three objects are members of Virgo. The choice of the parameter p_{ext} for those galaxies sharing the same environment should be made consistent with the presence of a common intracluster medium and with the available observations. For example, *Ginga* (Awaki et al. 1991, Ikebe et al. 1992) and *Rosat* data (Böhringer et al. 1994) suggest a temperature T_{ext} in excess of ~ 2 keV for the intracluster medium in Fornax and Virgo.

The basic properties of the best fit stellar dynamical models adopted in the following study are summarized in Table 2. As shown by BPS, even if the stellar dynamical data are far from identifying a unique global model for the optical galaxy, it is sufficient to focus our attention on the best fit model for the mass distribution provided by stellar dynamics, since other models compatible with the same set of stellar dynamical data are not expected to produce significant changes in the cooling flow modeling.

In general, the models contain significant amounts of dark matter, as shown by Figure 1, which illustrates

the profiles of the cumulative mass-to-light ratio for each galaxy. Table 2 lists the mass-to-light ratio $M_\star/L_B$ for the luminous component and the total mass-to-light ratio M/L_B. The total luminosities given in the Table are taken from SBS. There is a wide range in the lengthscales r_L (the half-mass radius for the luminous component) and r_D (same, but for the dark matter), ranging from $r_L = r_D = 13$ kpc for NGC 1404 to $r_L = 28$ kpc, $r_D = 165$ kpc for NGC 4636 (columns 4 and 7 in the Table). Significant differences are also noted in the value of the (one-dimensional) central stellar velocity dispersion $\sigma_\star(0)$ (column 8). The galaxy M/L_B ratio and the scale length of the *total* mass distribution influence the steepness of the X-ray emission profile, while the central gas temperature depends upon the depth of the potential well, i.e., on the value of $\sigma_\star(0)$. So we would expect that objects with a concentrated mass distribution, like NGC 1404 and NGC 4374, have a less extended X-ray halo than 'giants' like NGC 1399 or NGC 4636. Furthermore, as a result of its relatively low velocity dispersion, NGC 1404, which is embedded in the X-ray halo of NGC 1399, should appear as a *cold* X-ray source relative to its environment; the opposite should occur for NGC 4374.

Finally, consider the values of L_X/L_B (see last column of Table 1). Even for this selected sample of bright E galaxies there is a very large spread (a factor 18 between NGC 1399 and NGC 4374). Within the cooling flow description, such a wide spread may just reflect a different accretion rate from the intracluster medium; in particular, NGC 1399 is expected to accrete large amounts of hot gas from its surroundings. This point is discussed further in the next section.

3. THE METHOD.

We describe the hot coronal gas by means of a standard set of equations under the assumption of a steady-state, spherically symmetric inflow in the presence of mass and energy source terms (related to mass and energy injection in the form of hot gas originating from stars and supernovae), of radiative losses (responsible for the observed X-ray emission), and of a mass sink term (describing the decoupling of cold gas from the hot phase; Sarazin & Ashe 1989):

$$\frac{1}{r^2}\frac{\mathrm{d}}{\mathrm{d}r}(r^2\rho u) = \alpha\rho_\star - q\frac{\rho}{\tau_{dec}} \tag{1}$$

$$\rho u\frac{\mathrm{d}u}{\mathrm{d}r} + \frac{\mathrm{d}p}{\mathrm{d}r} = -\rho\frac{\mathrm{d}\Phi}{\mathrm{d}r} - \alpha\rho_\star u \tag{2}$$

$$\frac{1}{r^2}\frac{\mathrm{d}}{\mathrm{d}r}\left[r^2\rho u\left(\frac{1}{2}u^2 + \frac{5}{2}\frac{p}{\rho} + \Phi\right)\right] = \\ = -\rho^2\Lambda(T) + \alpha\rho_\star\left(\epsilon_{inj} + \Phi\right) - q\frac{\rho}{\tau_{dec}}\left(\frac{1}{2}u^2 + \frac{5}{2}\frac{p}{\rho} + \Phi\right). \tag{3}$$

These equations reduce to the same set used by BPS when $q = 0$. Three unknown functions ρ, p, and u (mass density, pressure, and radial velocity) describing the hot, X-ray emitting gas are to be derived by solving the above equations under the appropriate boundary conditions (see below). The gas temperature T is obtained from the equation of state $p = \rho kT/\mu m_p$. Note that we are ignoring the contribution of the possible presence of magnetic fields and of various transport processes within the gas. In the following, we will refer to the solutions of this set of equations as "q-models".

(i) *Input parameters for the hot gas*

The chemical composition of the gas is assumed to be "cosmic" (Allen 1973), with a mean mass per particle $\mu = 0.63$ in units of the proton mass m_p. The quantity $\alpha = 4.75 \times 10^{-19} (M_\star/L_B)^{-1}$ sec^{-1} (with the mass–to–light $M_\star/L_B$ ratio expressed in solar units) is the rate of mass loss of a 15 Gyr old stellar population that is taken to be "quiescent" (i.e., with no significant star formation after the initial stage), as given by Renzini (1988). The specific energy of the injected material is derived from $\epsilon_{inj} = \frac{3}{2}(\sigma_\star^2 + \vartheta_{SN} \varepsilon_{SN} \frac{k\hat{T}_{SN}}{\mu m_p})$. Here $\sigma_\star$ is the one-dimensional stellar velocity dispersion (averaged over the three directions), taken from the stellar dynamical model, ϑ_{SN} is the SNIa rate relative to Tammann's (1982) value (0.22 SNIa per century per $10^{10} L_{\odot B}$), ε_{SN} is the mechanical energy released in a SNIa explosion normalized to 10^{51} erg, and $\hat{T}_{SN} = 2.8 \times 10^7$ ^{0}K is an effective temperature associated with the hot supernova ejecta mixing into the gas. Our reference case will be characterized by $\vartheta_{SN} = 1/4$ (see Cappellaro et al. 1993) and $\varepsilon_{SN} = 1$, but we will explore also the regime of very low supernova rate $\vartheta_{SN} = 1/16$, for which the heating is typically dominated by the stellar contribution, and the regime of high supernova rate, $\vartheta_{SN} = 1.1$, where the heating is generally supernova dominated.

The cooling function $\Lambda(T)$ is obtained by numerical interpolation of the results of Raymond, Cox & Smith (1976), and is suitable for an optically thin thermal plasma with cosmic abundances at temperatures 10^5 ^{0}K $< T < 10^8$ ^{0}K.

(ii) *The mass decoupling term*

Following the physical prescription of Sarazin & Ashe (1989), we describe the decoupling of cold material from the hot gas by referring to the timescale

$$\tau_{dec} = \frac{5}{2} \frac{p}{\rho^2 \Lambda(T)} \left(2 - \frac{\mathrm{d}\ \ln\Lambda}{\mathrm{d}\ \ln T} \right)^{-1} = \tau_{cool} \left(2 - \frac{\mathrm{d}\ \ln\Lambda}{\mathrm{d}\ \ln T} \right)^{-1} \tag{4}$$

which is the linear growth rate of the thermal instability for comoving, isobaric density perturbations to the smooth ('homogeneous') flow (Mathews & Bregman 1978). In contrast to the injected mass from the stars, the decoupled cold material is assumed not to exchange momentum or entropy with the hot gas. The dimensionless parameter q appearing in the continuity equation is considered to be as a free (phenomenological) constant parameter of the model, to be determined by the fit process. Note that the decoupling time given above differs from that of most models by Sarazin & Ashe (1989) (hereafter "q_S–models") by a factor

$$c(T) = \left(2 - \frac{\mathrm{d}\ \ln\Lambda}{\mathrm{d}\ \ln T} \right), \tag{5}$$

which ranges from 2.0 to 3.9 when T ranges from 0.5 to 1.5 keV. Because of this temperature dependence, the q_S-models behave as q-models with a *differential* $q = q(r)$. In practice, q_S–models with $q_S = 3q$ and with the values of p_{ext} and $\dot{m}_{ext}$ suggested by our best-fit models for NGC 1399, NGC 4472 and NGC 4636, are found to differ only slightly from the corresponding q-models.

(iii) *The stellar component and the gravitational potential*

The three functions $\rho_\star(r)$, $\sigma_\star(r)$, and $\Phi(r)$ are the *stellar* mass density, the one-dimensional stellar velocity dispersion (averaged over the three directions), and the gravitational potential of the galaxy (with the contribution of stars and dark matter, but, for simplicity, *without* the contribution of the gas) derived from the best-fit stellar dynamical models described in §2.

(iv) *Boundary conditions and integration scheme*

Equation (1) is integrated to give for the inward mass–flux $\dot{m}$:

$$\dot{m} = -4\pi r^2 \rho u = \alpha \left[M_\star(r_{ext}) - M_\star(r) \right] - q \left[D(r_{ext}) - D(r) \right] + \dot{m}_{ext}, \tag{6}$$

where $M_\star(r)$ is the galactic *stellar* mass inside a sphere of radius r, and $D(r) = \int_0^r \frac{\rho}{\tau_{dec}} 4\pi r^2 \mathrm{d}r$. The sign of $\dot{m}$ is chosen so that it is positive for an inflow. The quantity $\dot{m}_{ext}$ is the

contribution to the flux due to accretion of external gas. Its value sets one boundary condition at r_{ext}. For the models shown in §4 , r_{ext} is chosen to be equal to R_X (see Table 1). Note that in some objects (like NGC 4374) this radius may fall within the optical galaxy. A second boundary condition is that the pressure at r_{ext} be $p = p_{ext}$. The two quantities $\dot{m}_{ext}$ and p_{ext} are, like q, free parameters of the model. The third boundary condition is provided at the free boundary $r = r_s$ ('sonic radius'), defined as the radius at which $u = -\sqrt{5p/3\rho}$, where the derivatives of the unknown functions ρ, u, p are required to be finite. This latter condition implies

$$\rho^2 \Lambda(T) \left[1 + q\left(2 - \frac{\mathrm{d}\ln\Lambda}{\mathrm{d}\ln T}\right)\right] + \frac{3}{2}\rho u\left(-\frac{\mathrm{d}\Phi}{\mathrm{d}r} + 2\frac{u^2}{r}\right) - \alpha\rho_\star(r)(\epsilon_{inj} + 2u^2) = 0 \tag{7}$$

at $r = r_s$.

The integration is started at a guess for r_s, where the mass flux is specified in terms of the parameter ϵ, defined as

$$\epsilon = \frac{\dot{m}(r_s)}{\alpha\left[M_\star(r_{ext}) - M_\star(r_s)\right] + \dot{m}_{ext}}, \tag{8}$$

which is the gas mass fraction at the sonic radius r_s which has 'survived' the decoupling process. In the case $q = 0$, Eq. (1) is integrated trivially, with the parameter ϵ equal to 1. In the opposite limit of large q, ϵ becomes vanishingly small. The values of r_s and ϵ are varied and the integration iterated until the mass flux $\dot{m}$ and the pressure p at $r = r_{ext}$ are found to match the specified values of $\dot{m}_{ext}$ and p_{ext}. Alternatively, when the value of r_s is seen to shrink below 0.1pc, so that ϵ also becomes very small, a fully subsonic solution is looked for. The integration is then carried inward from r_{ext} starting with a guess for $\rho(r_{ext})$ which is improved, for fixed $\dot{m}_{ext}$ and p_{ext}, until the central mass flux becomes vanishingly small. The numerical code employed (Toniazzo 1993) uses a double shooting integration scheme with a variable-step fourth-order Runge-Kutta integrator. In the case $q = 0$, a simple shooting method from r_s outward is found to be viable. When $q \neq 0$, such simple shooting method becomes unstable.

The models illustrated in §4 have been chosen with the following procedure. For a given galaxy, several models with different parameters have been calculated, with the goal of fitting the emission profile and of matching the value of the integrated luminosity. At a second stage, attention was given to the published constraints on the temperature. The models are quite sensitive to the values of q and $\dot{m}_{ext}$, and less to p_{ext}.

The code has been tested by checking against the results of BPS, for the $q = 0$ model of NGC 4472, and the results presented by Sarazin & Ashe (1989).

(v) *Properties of the q–models*

In the construction of the "q-models", we may take advantage of the fact that the values of p_{ext} and $\dot{m}_{ext}$ have a definite 'plausibility' range. It should be stressed that p_{ext} and $\dot{m}_{ext}$ influence only the outer profiles, while for radii smaller than the optical radius R_e the major role is played by q, by the adopted gravitational potential Φ (which in particular determines the central temperature, in the transsonic part of the flow), and by the adopted supernova rate.

For a given distance to the observed object, the measured X-ray surface brightness and temperature at large radii suggest a value for the pressure of the gas p_{ext}. In particular, *Rosat* data may be able to constrain this quantity for many objects (see, e.g., Trinchieri et al. 1994). For models where q plays a significant role, the amount of gas accreted from the cluster or from the group can be estimated as follows. The mass continuity equation (Eq. 1) evaluated at r_s can be rewritten as:

$$\frac{\dot{m}_{ext}}{\alpha M_\star} = \frac{q\left[D(r_{ext}) - D(r_s)\right]}{(1-\epsilon)\,\alpha M_\star} - \delta, \tag{9}$$

with $\delta \approx 1$. Since r_s is very small in our models, it may effectively be replaced by 0, so that the D–terms are related to the *total* radiated power

$$L_t = \int_0^{r_{ext}} \rho^2 \Lambda\left[1 + qc(T)\right] 4\pi r^2 \mathrm{d}r. \tag{10}$$

Then the continuity equation yields the following estimate for the accretion rate

$$\frac{\dot{m}_{ext}}{\alpha M_\star} \approx \frac{1}{1-\epsilon}(\frac{0.7L_t}{L_X})\left\langle \frac{4qc(T)}{1+qc(T)}(\frac{1\mathrm{keV}}{kT})\right\rangle \frac{(L_X/10^{41}\mathrm{erg\ s^{-1}})}{(L_B/10^{10}\mathrm{L_\odot})} - 1, \tag{11}$$

where the angular brackets denote average over the *total* (bolometric) emission. Both the numerator and the denominator in Eq.(11) go to zero when $q \to 0$, so this equation is not useful in this limit. In such limiting case $\dot{m}_{ext}/\alpha M_\star$ has to be estimated directly from the energy equation that can be derived by integrating Eq.(3). In practice, all the models selected in the following are in the regime of finite q, with $q \geq 0.1$ and $\epsilon < 0.1$.

The quantity L_X denotes the power radiated in the relevant X-ray band. Following Sarazin & Ashe (1989), this can be obtained from the specific emission

$$b_X(r) = \rho^2 \Lambda_X(T)\left[1 + qc(T)\frac{\Lambda(T)}{\Lambda_X(T)}\int_0^T \frac{\Lambda_X(T')}{\Lambda(T')}\frac{\mathrm{d}T'}{T}\right], \tag{12}$$

where Λ_X is the emission in the *Einstein* $0.5 - 4.0$ keV energy band. The emission spectrum is assumed to be that computed by Raymond & Smith (1977) for a thermal plasma with "cosmic" (Allen 1973) abundances. Note the q–dependence of $b_X(r)$, which thus includes the contribution of the cooling gas that gets decoupled from the hot phase. Therefore, the fraction of power radiated in the X-ray band L_X/L_t for the model of interest depends both on the temperature distribution and on the value of q. For the selected models of the following §4, this fraction ranges from 0.57 to 0.70.

If the heating due to supernovae dominates over other energy sources, the close similarity of the light profile and the X-ray emission profile in the inner parts of X-ray bright galaxies displayed by existing *Einstein* HRI data is found to occur naturally in models characterized by $q \gg 1$ (Sarazin 1990). In practice, the value of $q \approx 1.3$ turns out to mark the transition to this asymptotic behavior. As will be shown below, good fits are obtained to the relevant profiles for $q \approx 0.5$.

4. THE MODELS

Three sets of models are presented, corresponding to three different assumptions on the SNIa rate: $\vartheta_{SN} = 1/16, 1/4$, and 1.1. Tables 3, 4, and 5 summarize the main global parameters of the models in each case.

For each model we compute several profiles. Some profiles are specifically produced for comparison with the observations (see Figs. 2, 3, and 4 corresponding to the three different assumptions on the SNIa rate). The model X-ray surface brightness $\Sigma_X(R)$ at projected distance R is computed by integrating the quantity b_X of Eq.(12) over the line-of-sight line element $d\ell$. For those cases where comparison is made with *Einstein* IPC and *Rosat* PSPC data, the surface brightness profiles are convolved with gaussians of 110" and 60" FWHM respectively. The fit process to the observed surface brightness data is especially aimed at reproducing the *shape* of the observed profiles. The data points shown in the Figures are treated by allowing for a modest adjustment of the conversion factor from count rates (given by the original data sources) to the physical units. In the following, when we will talk about "overbright" models we will mean those for which the model X-ray luminosity exceeds significantly value for L_X of Table 1.

The projected emission temperature is computed from

$$T_X(R) = \frac{\displaystyle\int d\ell\ \rho^2 \Lambda_X(T) T\left[1 + qc(T)\frac{\Lambda(T)}{\Lambda_X(T)}\int_0^T \frac{\Lambda_X(T')}{\Lambda(T')}\frac{\mathrm{T'dT'}}{T^2}\right]}{\Sigma_X(R)}, \tag{13}$$

which is an emission-weighted temperature of the gas. [Note that the weight entering the integral over the line-of-sight slightly differs from $b_X(r)$ in the term that describes the contribution of the decoupled gas.] In the Tables we report for each model the value of an emission averaged (i.e., based on $\Sigma_X(R)$, over the whole galaxy) temperature $\langle kT \rangle$. In general, this latter quantity is different from the temperature that could be derived from a best–fit to the emitted radiation by a Raymond spectrum. The result of this fit depends on the sensitivity of the instrument as a function of photon energy; in particular, it will be biased towards the peak of the detector quantum efficiency. Figure 5 shows more in detail the emission profiles of the three brightest objects, comparing the results of models obtained for different assumed SNIa rates. The profiles of some physical quantities (temperature $T(r)$, particle density $n(r) = \rho(r)/\mu m_p$ and mass flux $\dot{m}(r)$), describing the intrinsic properties of the models, are shown in Fig. 6.

(i) *Global properties of the selected models*

If we exclude the case of NGC 1404, which turns out to be a peculiar object in this modeling context (see comments below), the selected models are characterized by a fairly uniform value of q which decreases smoothly when the assumed value of ϑ_{SN} is increased.

The model accretion rates $\dot{m}_{ext}$, which are smaller for higher assumed values of ϑ_{SN}, show a wide variation from galaxy to galaxy. The models for NGC 4374 all have a nominal value of 0.1 $M_\odot$/yr. For NGC 4472, $\dot{m}_{ext}$ ranges from 1 $M_\odot$/yr to 0.3 $M_\odot$/yr. The latter value refers to the overbright model with $\vartheta_{SN} = 1.1$; in this case, a lower accretion rate would not be compatible with the existing surface brightness and temperature data at large radii. The accretion rates in NGC 1404 are not large, but $\dot{m}_{ext}$ is significant when the adopted supernova rate is small. In contrast, for any of the assumed choices of ϑ_{SN}, most of the gas present in NGC 4636 is found to originate from the outside (about 67% for the lowest value of the supernova rate). The energetics of NGC 1399 appears to be dominated by a substantial accretion of external gas.

The values of the external pressure p_{ext} identified by our modeling procedure are on the high side, ranging from 4×10^3 ^{0}K cm^{-3} to 1.5×10^4 ^{0}K cm^{-3}. The latter value refers to NGC 4374 for a high assumed supernova rate; lower values of p_{ext} would also give reasonable models for this galaxy. In general, these relatively high values of p_{ext} are produced in order to fit a fairly flat surface brightness profile in the outer parts and are consistent with the overall increase in the temperature profiles in the outer regions suggested by the existing data (see also Böhringer et al 1994).

We should stress that the high value of $\vartheta_{SN} = 1.1$ suggested by van den Bergh & Tammann (1991) would imply that the energy input is dominated by supernovae. This explains why the corresponding selected models tend to be characterized by larger pressures p_{ext} (especially for the objects with small r_{ext}) and by smaller accretion rates $\dot{m}_{ext}$. Note that, in the case of high supernova rate, the selected models for NGC 4374 and NGC 4472 are overbright, by factors of 2.4 and 1.4 respectively.

The mass of the gas M_{gas} recorded in the Tables gives the integral of ρ out to r_{ext}. The numbers here are found to be quite large compared to previous estimates (see Forman et al. 1985, Thomas et al. 1986). This is particularly true for NGC 1399 and NGC 4636, for which the mass of the hot gas is of the same order as that of the stellar component. One obvious worry is that, under these conditions, the self-gravity of the gas should be incorporated in the model. Fortunately, the models do have sizable amounts of dark matter, so that even in the worst case (model $\vartheta_{SN} = 1/16$ for NGC 1399) the gas actually makes up no more than 6% of the *total* mass inside r_{ext} (this percentage drops to 3% for NGC 4636, 2% for NGC 4472 and NGC 1404 and less than 1% for NGC 4374).

NGC 1404, as might have been anticipated, turns out to be somewhat peculiar. Its peaked emission profile and its large L_X/L_B require a small value for the parameter q (0.1), independently of the assumed supernova rate (however, the $q = 0$ models are ruled out). The cooling flow models for this object also stand out because

of their relatively flat $\dot{m}$ profiles (see further discussion in item (iii) below). It appears that the characteristics of this galaxy mostly result from the interaction with its environment, dominated by NGC 1399. From the point of view of the observational input, one has to face a non–trivial subtraction problem, since the galaxy is embedded in the bright halo of NGC 1399. The models adopted are clearly oversimplified with respect to the actual physical situation. Still we find no particular difficulty in fitting the emission profile of NGC 1404. In view of its shallow potential well and of the constraints posed on p_{ext} by the apparent proximity to NGC 1399, a relatively low average X-ray emission temperature (≈ 0.6 keV) is predicted for the hot gas.

¿From the properties of the environment identified by our models, it turns out that the intergalactic medium in Virgo and Fornax should be characterized by relatively high densities, so that ram–pressure stripping may be expected to be efficient. This is indeed suggested by White and Sarazin (1991), who find a correlation between the dispersion in L_X for a given L_B and the local number density of galaxies. On the other hand, the effectiveness of ram–pressure stripping largely depends on the velocity of the galaxy relative to the medium (Gaetz et al. 1987). In particular, for typical values of $\rho(r_{ext})$ in our models (10^{-3} amu), the condition for efficient stripping (see Eq.(10) in White and Sarazin 1991) does not seem to be satisfied for velocities below 500 km/s. Indeed, the X-ray isophotes of NGC 1399 and NGC 4636 are fairly round.

After submission of this paper, some interesting results from the *ASCA* mission have come to our attention (Loewenstein et al. 1994; Mushotzky et al. 1994), which may provide an additional way to discriminate our models, based on their average temperatures $\langle kT \rangle$ (see column 8 of Tables 3–5). For NGC 4636 the *ASCA* temperature measurements are consistent with those of Trinchieri et al. (1994) (based on *Rosat* data), which are accounted for in our models. For NGC 4374 and NGC 1404 the values of 0.74 and 0.75 keV seem to point in the direction of the choice $\theta_{SN} = 1/4$. For these two galaxies, a quick investigation has shown that models can be produced, characterized by average temperatures consistent with the *ASCA* values; in particular, in the case of NGC 1404 a model with $q = 0.2$, $\dot{m}_{ext} = 0.9 \mathrm{M}_\odot/yr$, $p_{ext} = 2.2 \times 10^4$ ^{0}K cm^{-3}, and $\theta_{SN} = 1/4$ gives $\langle kT \rangle = 0.79$ keV with a reasonable emission profile.

(ii) *Surface brightness and temperature profiles*

For four objects in our sample, both the emission and the temperature profiles compare well with the available *Einstein* IPC data. The case of NGC 4636 stands out because the photometric fit is unsatisfactory for both IPC and *Rosat* PSPC data. While the latter data are closer to the model profiles, they also show a clear lack of circular symmetry; still the temperature profile is sufficiently well reproduced. The impact of the assumed supernova rate ϑ_{SN} is best noted in the innermost parts of the profiles, as shown in Fig. 5 (logarithmic scale) in comparison with HRI data. In the low ϑ_{SN} case, we find an excess of emission with respect to the innermost *Einstein* HRI data points for the galaxy NGC 4472; when a higher supernova rate is considered, the fit to the high resolution HRI data in the central regions definitely improves. No important changes in the emission and temperature profiles on the large scale are noted. For the case of high supernova rate ($\vartheta_{SN} = 1.1$), the model temperature profile of NGC 4636 is not fully satisfactory when confronted with *Rosat* PSPC data; this might be improved by allowing for a larger $\dot{m}_{ext}$, but in such a case the model would be overbright.

Figure 5 also shows the behavior of the best–fit model for the case $q = 0$ considered by BPS. This gives convincing evidence that the q–models are indeed able to remove almost completely the objection raised against simple cooling flow models in relation to the predicted emission profiles.

(iii) *Intrinsic profiles*

In Fig. 6 we summarize the properties of the intrinsic profiles that characterize the selected models.

For the three galaxies (NGC 1399, NGC 1404, and NGC 4636) with the highest values of $\dot{m}_{ext}/\alpha M_\star$, the accretion rate ($\dot{m}$) profiles are monotonically increasing; for NGC 1404 and NGC 4636, characterized by the

lowest model values of q, such profiles are relatively flat. For NGC 4374 and NGC 4472, the accretion rate is non–monotonic in the vicinity of r_{ext}.

¿From Fig. 6 one can see that our models are computed down to very small radii ($r < 10$ pc). The models are probably unphysical at such small galactocentric distances, but the profiles are shown in order to display the internal properties of the models and of the boundary conditions that have been adopted.

(iv) *Consistency of the steady-state cooling flow description*

In Fig. 7 we present the characteristic timescales for the models selected under the assumption of $\vartheta_{SN} = 1/4$. In each frame the three curves represent, as a function of galactocentric radius, the cooling timescale τ_{cool} (see Eq.(4)), the flow timescale (i.e., the time necessary for a fluid element to reach the center by moving at the fluid velocity $u(r)$), and the sound crossing time (i.e., the time necessary for a signal moving at the speed $u_s = -\sqrt{5p/3\rho}$ to reach the center). Models characterized by smaller values of q (as is the case of NGC 1404) tend to have smaller values of the flow timescale at r_{ext}.

¿From Fig. 7 one can see that the flow timescale actually exceeds the Hubble time in the outer parts of the flow (dashed lines). On the other hand, while the cooling time is even longer (solid lines), pressure equilibrium is guaranteed by the short ($\sim 10^8$yr, dotted lines) sound crossing time. We must conclude that the steady-state scenario is, strictly speaking, unjustified at very large radii; the calculated profiles are shown there also to describe the properties of the models at the outer boundary.

(v) *Some general trends from the selected sample of galaxies*

¿From the above discussion we find that, for a very low value of the supernova rate, the profiles are best fitted by models characterized by high values of q; still the central parts of the surface brightness profiles of the models are too steep. In contrast, based on $\theta_{SN} = 1.1$, the model temperature in the outer regions of NGC 4636 seems to be higher than that observed, while the model X–ray luminosities for NGC 4472 and NGC 4374 are in excess of the observed values by factors 1.4 and 2.4 respectively. The intermediate case ($\theta_{SN} = 1/4$) is probably the one to be preferred, if one assumes a strictly constant rate from galaxy to galaxy, although the innermost data point for the HRI profile of NGC 4472 is not well accounted for.

In our limited sample of galaxies, two potentially interesting correlations have been noted and are shown in Fig. 8. The right frame gives the correlation between $\dot{m}_{ext}/\alpha M_\star$ and $(L_X/10^{41}\mathrm{erg\ s^{-1}})/(L_B/10^{10}\mathrm{L_\odot})$:

$$\frac{\dot{m}_{ext}}{\alpha M_\star} \approx a\frac{(L_X/10^{41}\mathrm{erg\ s^{-1}})}{(L_B/10^{10}\mathrm{L_\odot})} - b. \tag{14}$$

A linear regression gives $a = 1.51, 1.53, 1.20$ and $b = -0.11, 0.11, 0.40$ (for $\vartheta_{SN} = 1/16, 1/4, 1.1$ respectively). This may be compared to the estimate given in Eq. (11). Thus a natural interpretation for the different L_X/L_B values that are observed in our sample of elliptical galaxies suggests that, because of dilution, the iron abundance in the hot gas of X-ray bright ellipticals should anticorrelate with L_X/L_B. The opposite trend would result if the higher L_X/L_B ratios were ascribed to higher SNIa rates, but this would be hard to justify.

In this scenario of a "diluted cooling flow" one would expect a metallicity gradient to be established preferentially for objects having high L_X/L_B. The decoupling of the gas from the cooling flow would enhance the effect. Clearly, a quantitative assessment of the actual dilution factor would require a full modeling of the history of the galaxy–cluster interaction, which is well beyond the limits of the steady–state analysis adopted in this paper. Such a detailed modeling would provide a determination of the size of the above mentioned metallicity gradient. At this stage we feel encouraged by the qualitative trends reported by Loewenstein et al. (1994) and Mushotzky et al. (1994).

Another possibly interesting trend that is noted is a fairly tight correlation between $\dot{m}_{ext}$ and the ratio r_h/r_L, where r_h denotes the half-mass radius of the *total* (dark + luminous) mass distribution of the galaxy.

Here the offset of NGC 1404 might be due to the peculiarities of this object pointed out above. While the X-ray emission and temperature profiles appear to be of modest significance in diagnosing the presence of dark halo in galaxies (see BPS), the total X-ray luminosity might be a significant indicator (see also Bertin et al. 1994). We recall that no other significant correlations of L_X/L_B with intrinsic galaxy properties have been noted (see White & Sarazin 1991).

5. CONCLUSIONS

We have shown that *within galaxy models constrained by radially extended stellar dynamical data*, a simple spherically-symmetric, steady-state, cooling-flow description with gas loss, generally compares well with the existing data on X-ray emission profiles and temperatures for a set of bright elliptical galaxies.

Three free parameters are needed to specify the model: (i) the external mass flux $\dot{m}_{ext}$, which represents accretion of intergalactic gas and increases the X-ray luminosity of the galaxy, (ii) the external pressure p_{ext}, which depends on the X-ray temperature of the cluster or group embedding it and helps confine the gas in the galactic potential well, and (iii) the dimensionless coefficient q, which parameterizes the decoupling of thermally unstable clouds of cooling gas from the homogeneous phase (Sarazin & Ashe 1989) and regulates the mass deposition rate along the flow.

Especially the use of the q parameter leads to significantly better fits to the X-ray emission profiles with respect to the $q = 0$ models, while the derived temperature profiles are consistent with, but only loosely constrained by, the existing data. Still it is evident that in some cases the assumption of spherical symmetry is an oversimplification; in addition, we must be aware that the steady-state condition is not fulfilled in the outer regions.

We have found that a value for the supernova rate in elliptical galaxies consistent with the estimate of Cappellaro et al. (1993) is favored by our models. Confining pressures of $p_{ext} \sim 4 \div 15 \times 10^3$ ^{0}K cm^{-3} and significant accretion rates of external material, up to $4 M_\odot$/yr, are suggested by our models. Finally, we have argued that the value of L_X/L_B should anticorrelate with the iron abundance in the gas inside ellipticals.

We would like to thank L. Ciotti, R. P. Saglia, C. L. Sarazin, and G. Trinchieri for valuable suggestions and for their collaboration. This work has been partially supported by ASI (under contract ASI 94 RS 94 – 202/3 FAE) of Italy.

Table 1. Optical and X-ray properties of the selected objects.

NGC	Type[7]	$D^{(8)}$ (Mpc)	$m_B^{(7)}$ (mag)	R_X (")	log L_X (erg/s)	$\langle T_X \rangle$ (keV)	$\log(L_X/L_B)^{(9)}$
1399	E1P	28	9.85	$1200^{(1)}$	$42.33^{(1)}$	$\geq 1.1^{(2)}$	31.46
				$120^{(3)}$	$41.63^{(3)}$	$1.02^{(3)}$	
1404	E1	28	10.87	$300^{(1)}$	$41.49^{(1)}$	$\geq 0.8^{(2)}$	31.10
				$220^{(4)}$	$41.36^{(4)}$	–	
4374	E1	27	9.98	$300^{(1)}$	$41.16^{(1)}$	$\geq 0.8^{(2)}$	30.20
				$150^{(5)}$	$40.84^{(5)}$	$0.9–1.3^{(5)}$	
4472	E2	27	9.09	$810^{(1)}$	$42.06^{(1)}$	$1.2^{(2)}$	30.73
				$\sim 200^{(3)}$	$41.77^{(3)}$	$0.92^{(3)}$	
4636	E0+	27	10.44	$600^{(1)}$	$41.99^{(1)}$	$0.9^{(2)}$	30.99
				$1080^{(6)}$	$42.27^{(6)}$	$0.87^{(6)}$	

(1) Fabbiano, Kim & Trinchieri 1992 (0.2–4.0 keV band)

(2) Kim, Fabbiano & Trinchieri 1992

(3) Serlemitsos et al. 1993 (0.5–4.5 keV band)

(4) Thomas et al. 1986

(5) Forman, Jones & Tucker 1985 (0.5–4.5 keV band). For the temperature a 90% confidence interval is reported.

(6) Trinchieri et al. 1994 (0.1–2.4 keV band). The temperature recorded here was computed as an emission weighted average.

(7) RC3 (de Vaucouleurs 1991)

(8) Faber et al. 1989

(9) L_X from column 6; L_B in solar units from SBS (see Table 2)

Table 2. Stellar–dynamical models (from SBS).

NGC	L_B ($10^{10}L_\odot$)	r_L (")	r_L (kpc)	$M_\star/L_B$ ($M_\odot/L_\odot$)	M/L_B ($M_\odot/L_\odot$)	r_D/r_L	$\sigma_\star(0)$ (km/s)
1399	7.5	136	18.4	8.0	58.0	6.2	250
1404	2.5	90	12.6	4.6	12.0	1.0	200
4374	9.2	179	23.5	5.3	14.2	1.0	308
4472	21.2	173	22.0	5.0	13.4	2.8	316
4636	9.9	215	28.1	8.0	38.6	5.9	227

Table 3: Properties of the selected models ($\vartheta_{SN} = 1/16$)

NGC	q	$\dot{m}_{ext}$ ($M_\odot$/yr)	p_{ext} (10^3 ^{0}K/cm^3)	r_{ext} (kpc)	M_{gas} ($10^{10}M_\odot$)	$\log(L_X)$ (erg/s)	$\langle kT \rangle$ (keV)	$\dot{m}_{ext}/\alpha M_\star$
1399	0.8	4.4	8.2	200	19.71	42.31	1.31	3.91
1404	0.1	0.9	10.0	50	0.69	41.41	0.52	2.40
4374	2.0	0.1	4.9	60	0.24	41.14	0.75	0.07
4472	0.8	1.0	10.1	120	4.42	42.02	1.09	0.31
4636	0.5	3.0	4.0	160	7.95	42.00	0.84	2.02

Table 4: Properties of the selected models ($\vartheta_{SN} = 1/4$)

NGC	q	$\dot{m}_{ext}$ ($M_\odot$/yr)	p_{ext} (10^3 ^{0}K/cm^3)	r_{ext} (kpc)	M_{gas} ($10^{10}M_\odot$)	$\log(L_X)$ (erg/s)	$\langle kT \rangle$ (keV)	$\dot{m}_{ext}/\alpha M_\star$
1399	0.6	4.1	7.6	200	19.55	42.29	1.24	3.65
1404	0.1	0.6	7.6	50	0.66	41.35	0.60	1.60
4374	0.8	0.1	6.3	60	0.51	41.35	0.85	0.07
4472	0.8	0.6	12.6	120	4.55	42.01	1.22	0.19
4636	0.4	3.0	3.8	160	8.20	42.02	0.80	2.02

Table 5: Properties of the selected models ($\vartheta_{SN} = 1.1$)

NGC	q	$\dot{m}_{ext}$ ($M_\odot$/yr)	p_{ext} (10^3 ^{0}K/cm^3)	r_{ext} (kpc)	M_{gas} ($10^{10}M_\odot$)	$\log(L_X)$ (erg/s)	$\langle kT \rangle$ (keV)	$\dot{m}_{ext}/\alpha M_\star$
1399	0.4	3.3	9.9	200	22.65	42.33	1.40	2.94
1404	0.1	0.3	8.9	50	0.65	41.33	0.67	0.80
4374	0.3	0.1	15.1	60	1.32	41.60	1.07	0.07
4472	0.3	0.3	12.6	120	6.00	42.14	1.17	0.09
4636	0.2	1.8	4.1	160	9.14	42.06	0.80	1.21

References

- Allen, C.W. 1973, Astrophysical Quantities, Athlone, London
- Awaki, H., Koyama, K., Kunieda, H., Takano, S., Tawara, Y., & Ohashi, T. 1991, ApJ 366, 88
- Balbus, S.A. 1988, ApJ 328, 395
- Bertin, G., Pignatelli, E., Saglia, R.P. 1993, A&A 271, 381 (BPS)
- Bertin, G., Bertola, F., Buson, L.M., Danziger, I.J., Dejonghe, H., Sadler, E.M., Saglia, R.P., de Zeeuw, P.T., and Zeilinger, W.W. 1994, A&A 292, 381
- Binney, J., Tabor, G. 1995, preprint
- Böhringer, H., Briel, U.G., Schwarz, R.A., Voges, W., Hartner, G., and Trümper, J. 1994, Nature 368, 828
- Cappellaro, E., Turatto, M., Benetti, S., Tsvetkov, D.Yu., Bartunov, O.S., Makarova, I.N. 1993, A&A 268, 472
- Ciotti, L., d'Ercole, A., Pellegrini, S., Renzini, A. 1991, ApJ 376, 380
- David, L.P., Forman, W., Jones, C. 1990, ApJ 359, 29
- de Vaucouleurs, G., de Vaucouleurs, A., Corwin, H.G., Jr., Buta, R.J., Paturel, G., Fouqué, P. 1991, "Third Reference Catalogue of Bright Galaxies", Springer, New York (RC3)
- Fabbiano, G., Kim, D.-W., Trinchieri, G. 1992, ApJS 80, 531
- Faber, S.M., Wegner, G., Burstein, D., Davies, R.L., Dressler, A., Lynden-Bell, D., Terlevich, R.J. 1989, ApJS 69, 763
- Fabian, A.C., Nulsen, P.E.J. 1977, MNRAS 180, 479
- Forman, W., Jones, C., Tucker, W. 1985, ApJ 293, 102
- Gaetz, T.J., Salpeter, E.E., Shaviv, G. 1987, ApJ 316, 530
- Ikebe, Y., Ohashi, T., Makishima, K., Tsuru, T., Fabbiano, G., Kim, D.-W., Trinchieri, G., Hatsukade, I., Yamashita, K., & Kondo, H. 1992, ApJL 384, L5
- Kim, D.-W., Fabbiano, G., Trinchieri, G. 1992, ApJS 80, 645
- Loewenstein, M. 1989, MNRAS 238, 15
- Loewenstein, M. 1990, ApJ 349, 471
- Loewenstein, M. 1992, ApJ 384, 474
- Loewenstein, M., Mathews, W.G. 1987, ApJ 319, 614
- Loewenstein, M., Mushotzky, R.F., Tamura, T., Ikebe, Y., Makishima, K., Matsushita, K., Awaki, H., Serlemitsos, P.J. 1994, ApJ 436, L75
- Lynds, R. 1970, ApJL 159, L151
- Mathews, W.G., Bregman, J.N. 1978, ApJ 224, 308

Murray, S.D., Balbus, S.A. 1992, ApJ 395, 99

Mushotzky, R.F., Loewenstein, M., Awaki, H., Makishima, K., Matsushita, K., Matsumoto, H. 1994, ApJ 436, L79

Pellegrini, S., Fabbiano, G. 1994, ApJ 429, 105

Raymond, J.C., Cox, D.P., Smith, B.W. 1976, ApJ 204, 290

Raymond, J.C., Smith, B.W. 1977, ApJS 35, 419

Renzini, A. 1988, in: Windows on galaxies, eds. G. Fabbiano, J.S. Gallagher, A. Renzini, Kluwer, Dordrecht, p. 255

Saglia, R.P., Bertin, G., Stiavelli, M. 1992, ApJ 384, 433 (SBS)

Saglia, R.P., Bertin, G., Bertola, F., Danziger, J., Dejonghe, H., Sadler, E.M., Stiavelli, M., de Zeeuw, P.T., Zeilinger, W.W. 1993, ApJ 403, 567

Sarazin, C.L. 1990, in: The Interstellar Medium in Galaxies, eds. H.A. Thronson, Jr. and J.M. Shull, Kluwer, Dordrecht, p. 201

Sarazin, C.L., Ashe, G.A. 1989, ApJ 345, 22

Sarazin, C.L., White, R.E. III 1987, ApJ 320, 32

Sarazin, C.L., White, R.E. III 1988, ApJ 331, 102

Sarazin, C.L., O'Connell, R.W., McNamara, B.R. 1992a, ApJL 389, L59

Sarazin, C.L., O'Connell, R.W., McNamara, B.R. 1992b, ApJL 397, L31

Serlemitsos, P.J., Loewenstein, M., Mushotzky, R.F., Marshall, F.E., Petre, R. 1993, ApJ 413, 518

Tammann, G. 1982, in: Supernovae, a Survey of Current Research, eds. M. Rees, R. Stoneham, Reidel, Dordrecht, p. 371

Thomas, P.A. 1986, MNRAS 220, 949

Thomas, P.A., Fabian, A.C., Arnaud, K.A., Forman, W., Jones, C. 1986, MNRAS 222, 655

Toniazzo, T. 1993, Tesi di Laurea, Universitá di Pisa

Trinchieri, G., Kim, D.-W., Fabbiano, G., Canizares, C.R. 1994, ApJ 428, 555

van den Bergh, S., Tammann, G. 1991, ARA&A 29, 363

Vedder, P.W., Trester, J.J., Canizares, C.R. 1988, ApJ 332, 725

White, R.E., Sarazin, C.L. 1991, ApJ 367, 476

Figure Legends

Figure 1. Cumulative M/L_B ratios for the best fit stellar dynamical models (from SBS) of the five elliptical galaxies of the sample. The models are made of a luminous component of total mass $M_\star$ and of a dark halo (with finite mass) with different spatial distribution, within a common self-consistent gravitational field. Thus the gradient in the cumulative $M = M(r)$ reflects the presence of a significant dark halo (see Table 2).

Figure 2. X-ray emission and temperature profiles for the selected models with $\vartheta_{SN} = 1/16$. *Left frames*: The solid lines are the model X-ray surface brightness profiles; the dotted lines (shown for all the objects with the exception of NGC 4472) are the result of a convolution with a gaussian PSF, suitable for a comparison with the IPC or PSPC data (see text). Triangles indicate *Einstein* IPC data (Fabbiano et al. 1992), crosses are used for the *Einstein* HRI data (for NGC 4472; Fabbiano et al. 1992) and bare errorbars are *Rosat* PSPC data (for NGC 4636; Trinchieri et al. 1994). *Right frames*: X-ray temperature profiles. The solid lines represent the projected emission temperature (see Eq. 13); the regions outlined by the dashed lines are the 90% confidence intervals derived from *Einstein* IPC data (Kim et al. 1992); errorbars are the temperature estimates derived by the *BBXRT* (for NGC 1399 and NGC 4472; Serlemitsos et al. 1993) and the *Rosat* PSPC (for NGC 4636; Trinchieri et al. 1994) instruments.

Figure 3. Same as Fig. 2, but for $\vartheta_{SN} = 1/4$ models.

Figure 4. Same as Fig. 2, but for $\vartheta_{SN} = 1.1$ models.

Figure 5. X-ray emission profiles for the brightest objects showing in detail the behavior in the innermost regions. The dotted lines refer to models with $\vartheta_{SN} = 1/16$, the short-dashed lines to $\vartheta_{SN} = 1/4$, and the long-dashed lines to $\vartheta_{SN} = 1.1$. Data points are *Einstein* IPC and HRI and *Rosat* PSPC data (as in Fig. 2). For NGC 4472 the dashed-dotted line showing the largest excess of emission in the central region corresponds to the FF model of BPS (with $q = 0$).

Figure 6. Intrinsic properties (temperature, particle density, and mass flux) of the selected models. As in Fig. 5, the dotted lines refer to models with $\vartheta_{SN} = 1/16$, the short-dashed lines to $\vartheta_{SN} = 1/4$, and the long-dashed lines to $\vartheta_{SN} = 1.1$.

Figure 7. Characteristic time scales in the cooling flows for the selected models with $\vartheta_{SN} = 1/4$. The solid lines represent the cooling times, the dashed lines the flow times, and the dotted lines the sound crossing times (see text).

Figure 8. Left panel: the mass accretion rate $\dot{m}_{ext}$ is found to be higher for diffuse halos (r_h is the half-mass radius of the *total* (dark + luminous) mass, while r_L is the half-mass radius of the luminous component). Right panel: scaling of the dilution parameter $\dot{m}_{ext}/\alpha M_\star$ with the relative X-ray luminosity $(L_X/10^{41}\mathrm{erg\ s^{-1}})/(L_B/10^{10}\mathrm{L_\odot})$. Here the values of the dilution parameter and of the luminosity L_X are taken from the selected models of Table 4 ($\vartheta_{SN} = 1/4$).

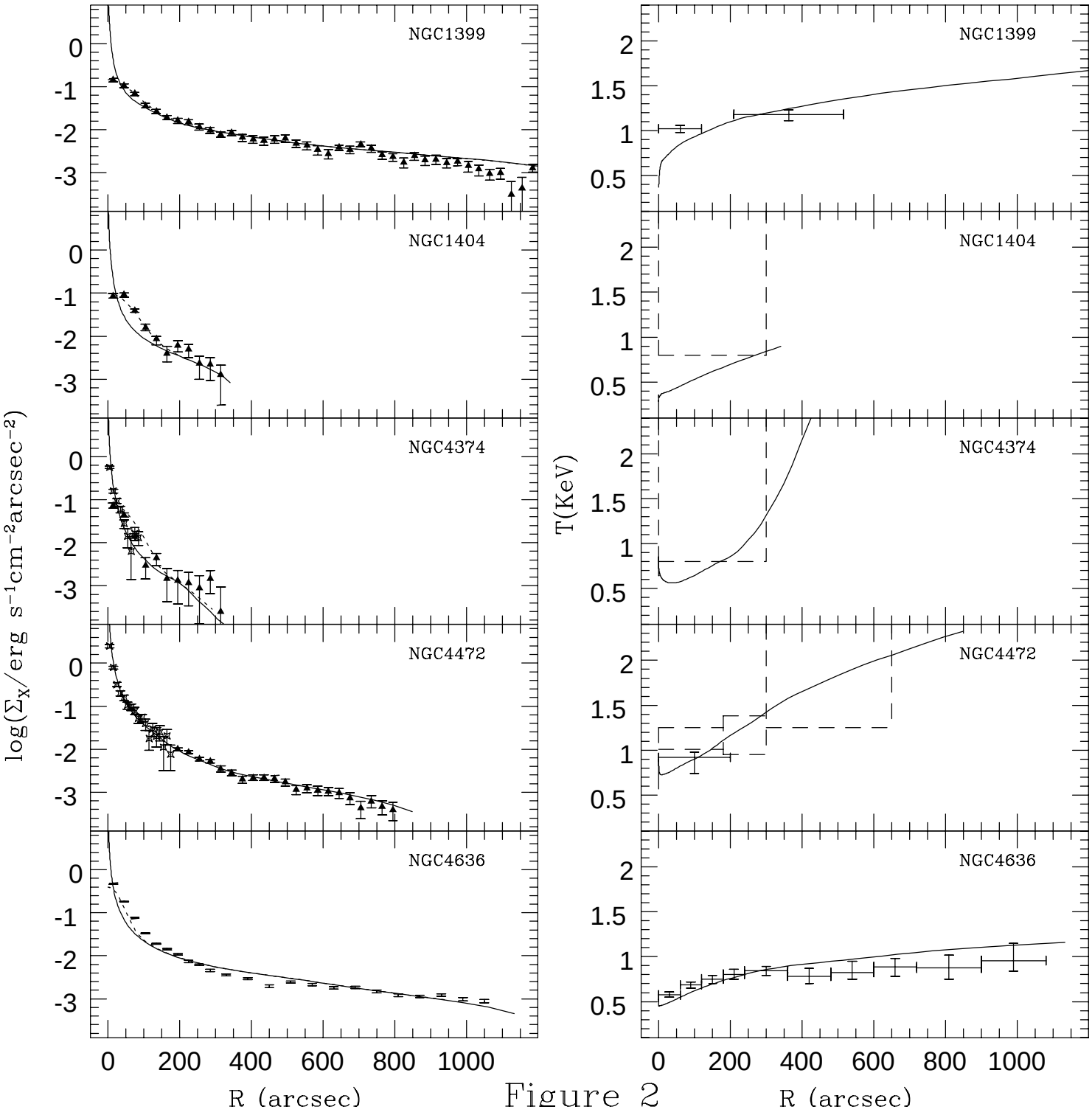
NGC1399
NGC1404
NGC4374
NGC4472
NGC4636
log(Σx/erg s-1cm-2arcsec-2)
T(KeV)
R (arcsec)
R (arcsec)

Figure 2

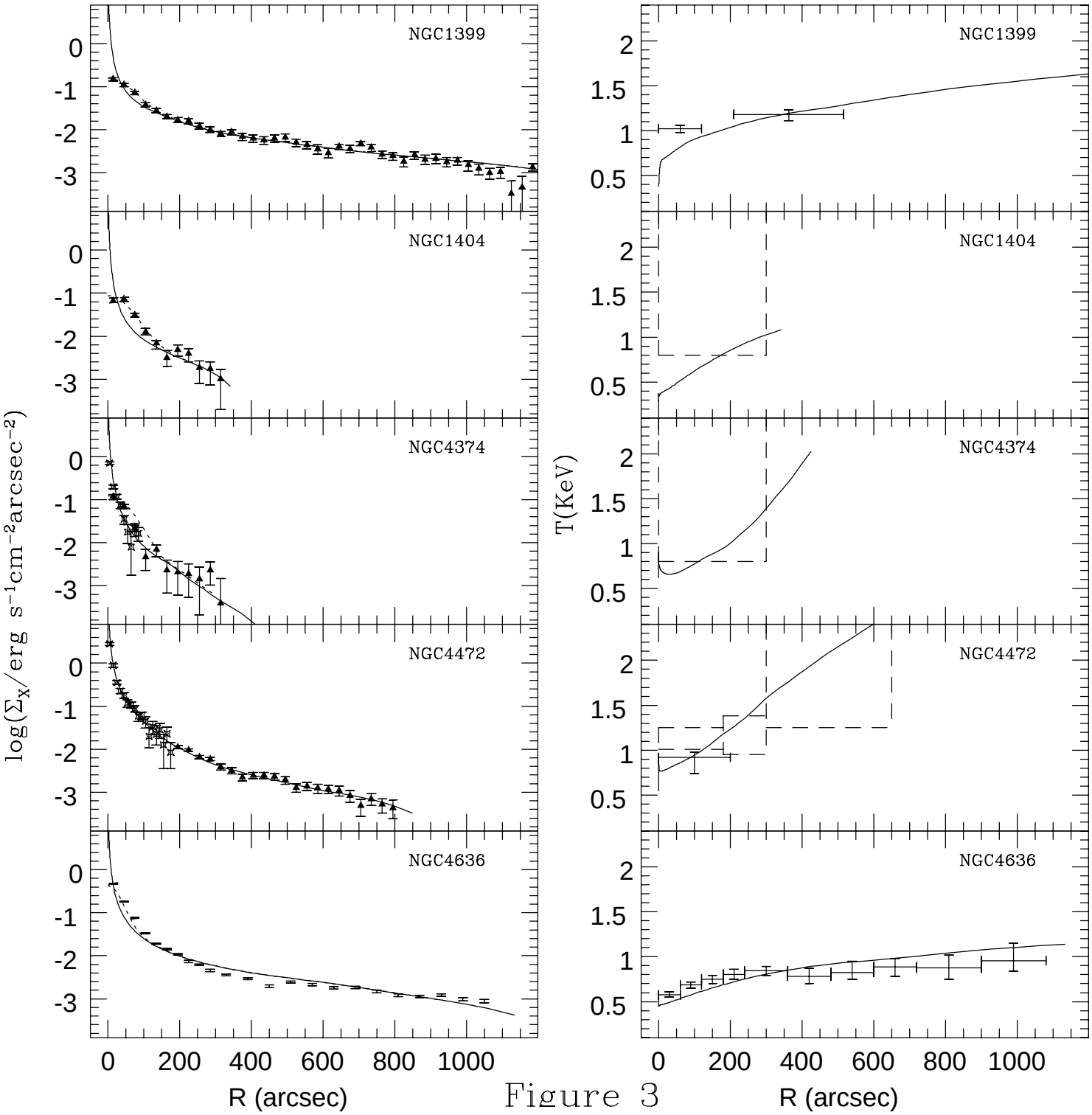
NGC1399
NGC1404
NGC4374
NGC4472
NGC4636
log(Σx/erg s⁻¹cm⁻²arcsec⁻²)
T(KeV)
R (arcsec)
R (arcsec)

Figure 3

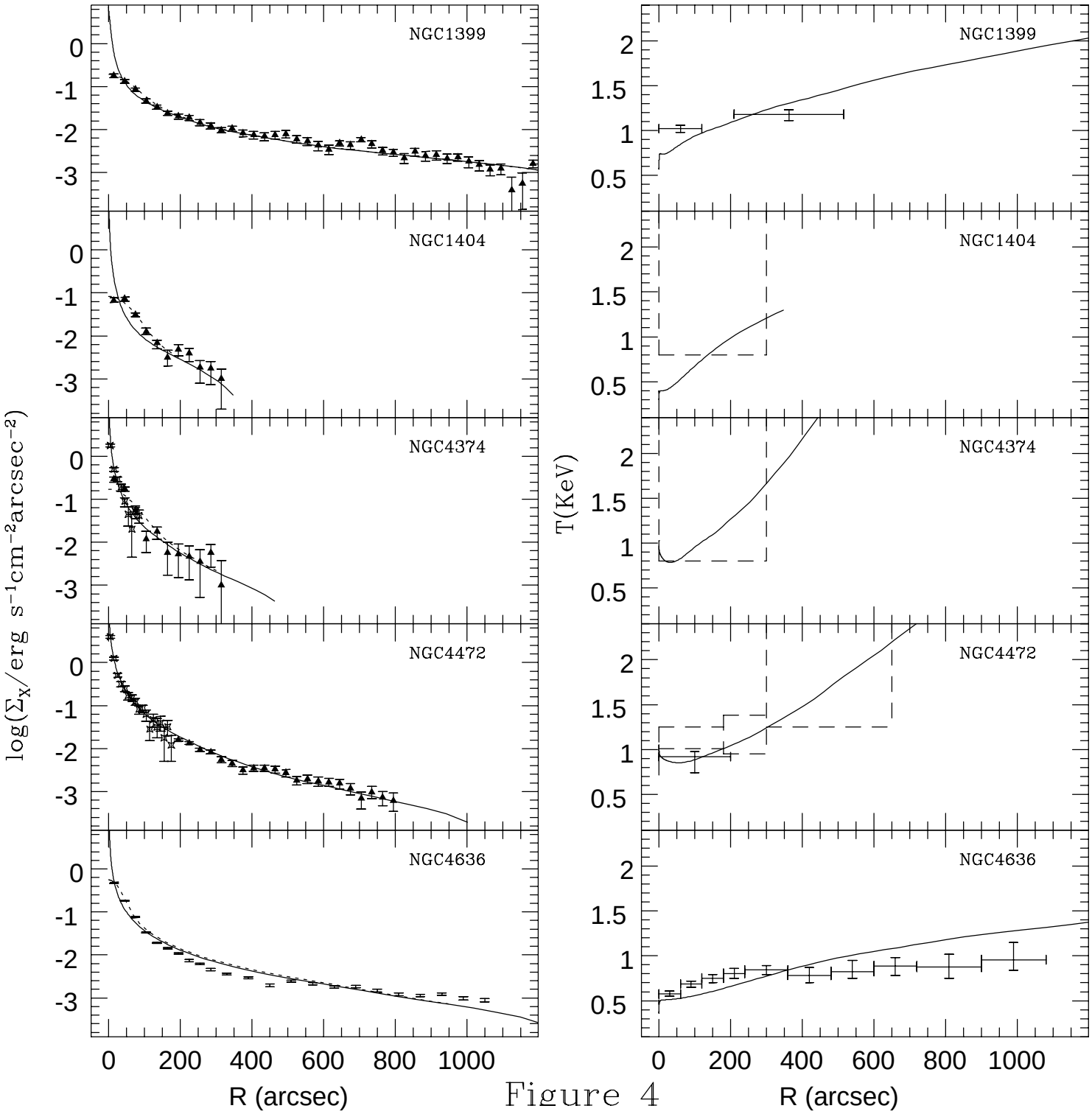
NGC1399
NGC1404
NGC4374
NGC4472
NGC4636
log(Σ_X/erg s^-1 cm^-2 arcsec^-2)
T(KeV)
R (arcsec)
R (arcsec)

Figure 4

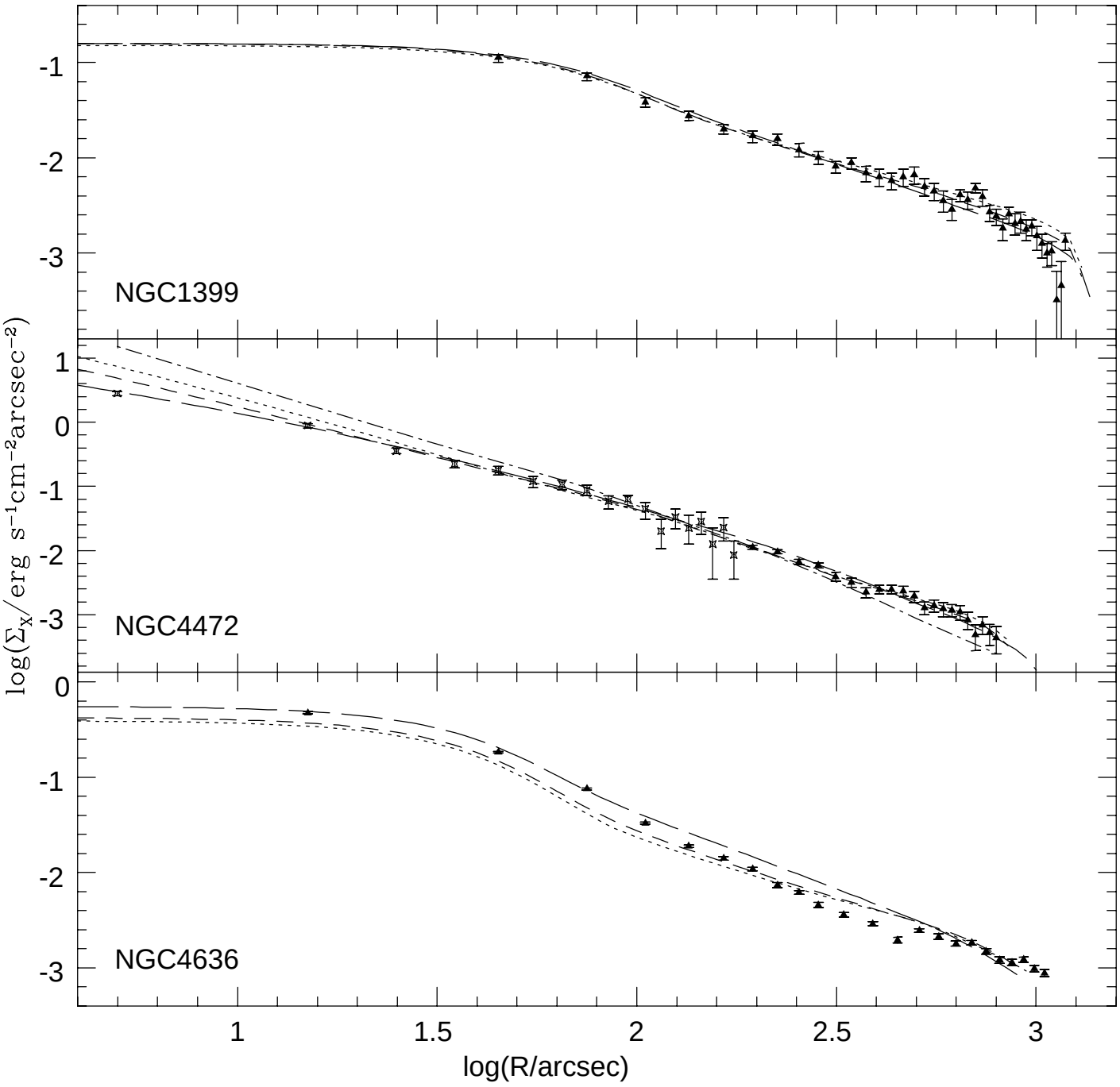
NGC1399
NGC4472
NGC4636
log(Σ_X/erg s^-1 cm^-2 arcsec^-2)
log(R/arcsec)
-1
-2
-3
1
0
-1
-2
-3
0
-1
-2
-3
1
1.5
2
2.5
3

Figure 5

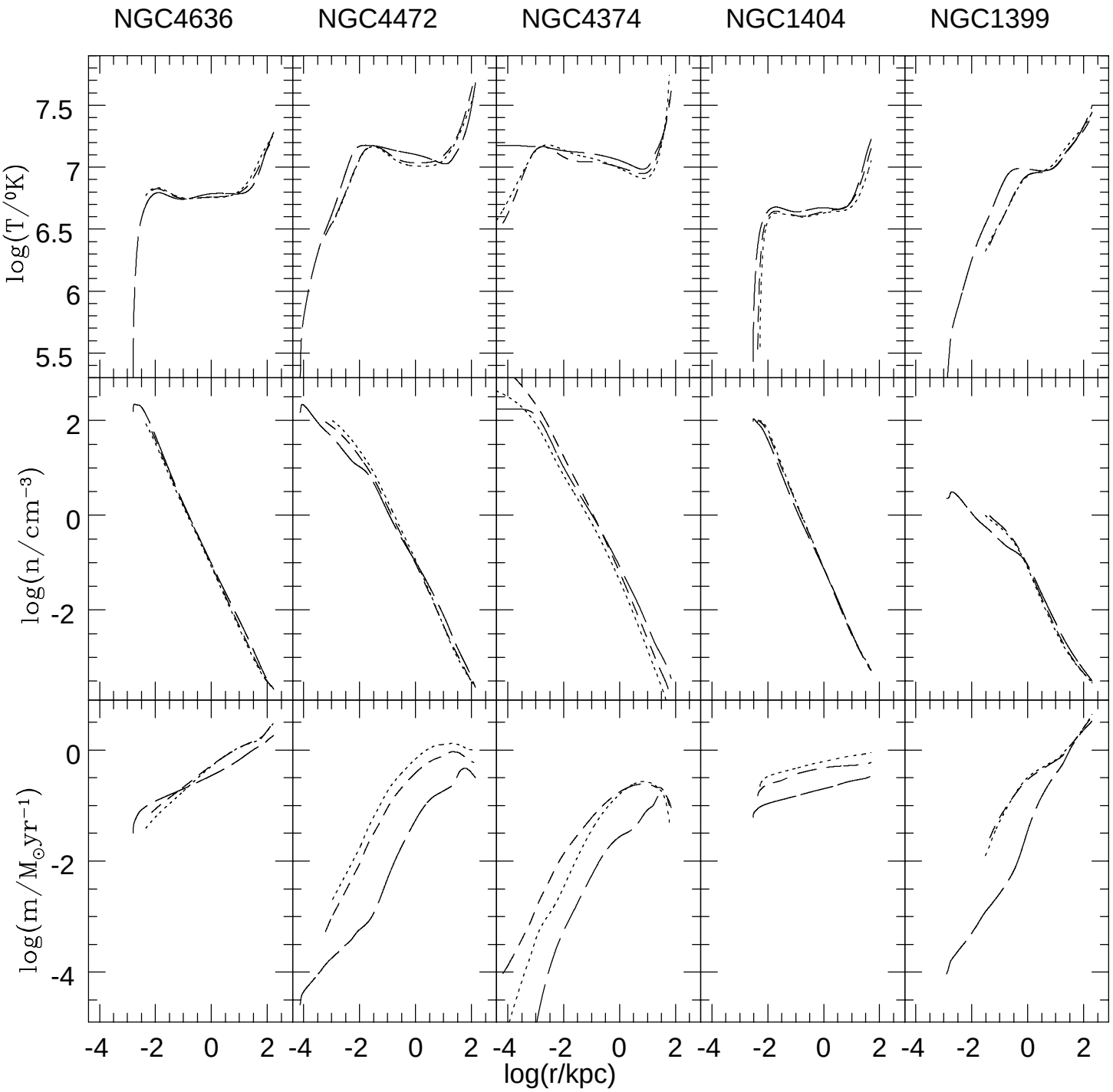
NGC4636
NGC4472
NGC4374
NGC1404
NGC1399
log(T/°K)
7.5
7
6.5
6
5.5
log(n/cm⁻³)
2
0
-2
log(m/M⊙yr⁻¹)
0
-2
-4
-4
-2
0
2
log(r/kpc)

Figure 6

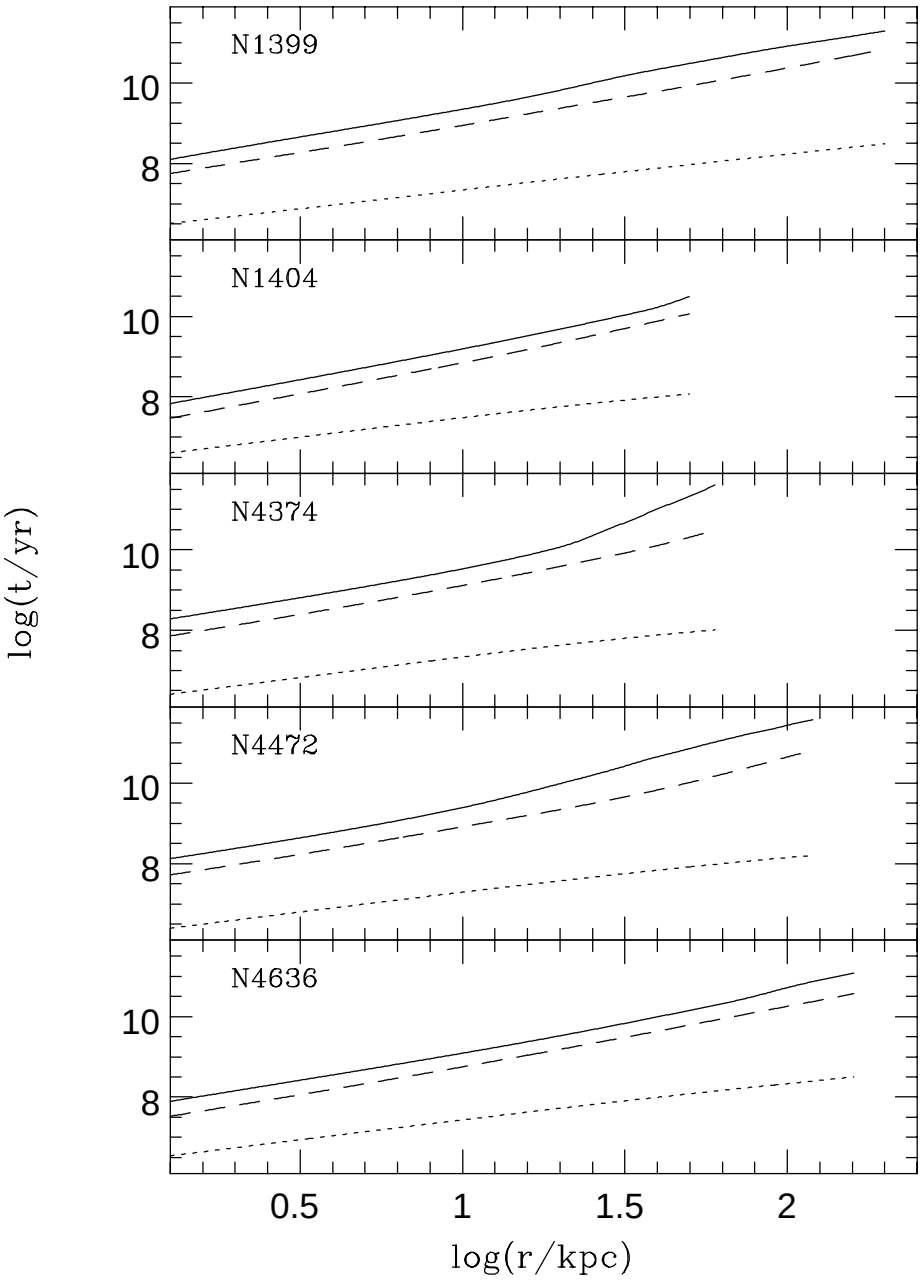

Figure 7

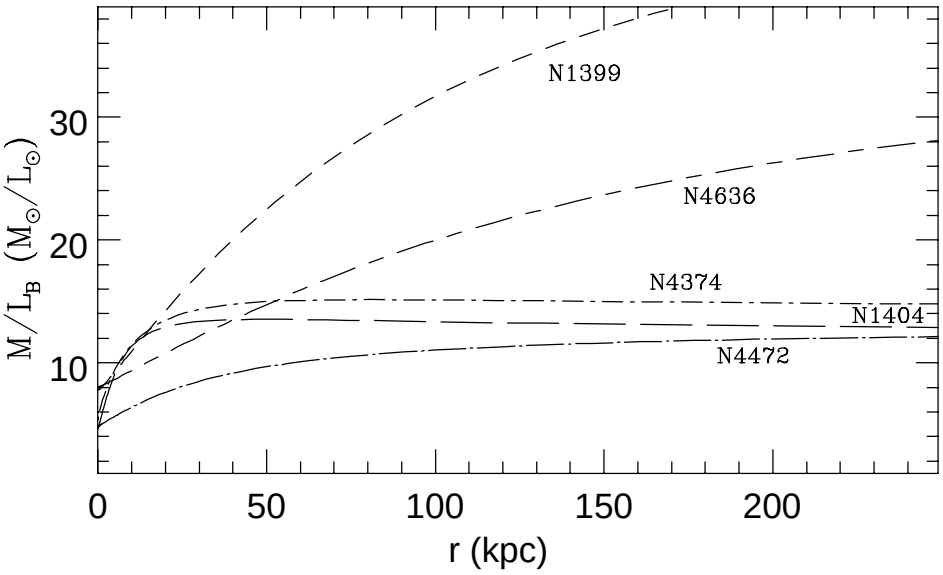

Figure 1

Figure 8